The International Journal of Advanced Manufacturing Technology (2019) 100:1931–1944
https://doi.org/10.1007/s00170-018-2787-y

ORIGINAL ARTICLE

Improving the weld microstructure and material properties of K-TIG welded armour steel joint using filler material

Zhenyu Fei [1,2] · Zengxi Pan [1,2] · Dominic Cuiuri [1,2] · Huijun Li [1,2] · Bintao Wu [1] · Lihong Su [1,2]

Received: 29 May 2018 / Accepted: 28 September 2018 / Published online: 11 October 2018

Abstract

Motivated by the undesired microstructure and unsatisfactory weld properties during keyhole tungsten inert gas (K-TIG) welding process, the use of filler materials was introduced for the first time in K-TIG to modify the weld microstructure and improve weld properties. Single pass full penetration was achieved on 6.2 mm armour steel plate at a welding speed of 350 mm/min. The metal transfer behaviour, microstructure and mechanical properties of weld joint were analysed in detail. The results showed that the introduction of filler material was very effective in modifying microstructure and improving joint properties. The wire feeding speed can reach up to 300 cm/min without compromising full penetration, providing a great scope for microstructure modification. The applied austenitic filler material can significantly change the weld microstructure with just 6.7% dilution, along with much increased weld metal hardness and joint efficiency, matching the welds produced by using conventional arc welding processes with V-joint preparation and matching filler metal. The introduction of filler material dramatically expands the capability of K-TIG process and also shows great potential to produce high performance armour steel joint with high productivity.

Keywords Keyhole welding · Tungsten inert gas welding · Filler material · Armour steel · K-TIG

1 Introduction

Armour grade quenched and tempered (Q&T) steels are widely applied in both military and non-military vehicle construction where resistance to projectile attack is highly desired, such as hull and turret of combat vehicles due to its high strength, hardness and high energy absorbing properties [1–3]. Welding and joining of such steel is unavoidable in the manufacturing process. At present, conventional fusion welding processes, such as gas metal arc welding (GMAW), or flux cored arc welding (FCAW) with either austenitic stainless steel or ferritic filler material are used to fabricate the weldment [4–6]. It is generally recognized that the harder the steel, the better the resistance to projectile attack [7]. The mechanical properties of the weldment are significantly decreased by the use of under-matching filler materials, especially the hardness in the weld metal region compared with base metal hardness, which results in much poorer ballistic performance.

Motivated by the significant loss of hardness in the weld metal region associated with under-matching filler materials, hardfaced interlayering with either chromium carbide or tungsten carbide deposit, combined with austenitic buttering as well as austenitic and/or ferritic capping have been introduced [8–11]. It has been reported that the ballistic performance was significantly improved provided that the design of the hardfaced interlayer and capping thickness was appropriate. However, the introduction of three different fillers produced inhomogenous weld microstructure, and the welding sequence was very complex. Also, the use of large amounts of hardfacing and austenitic filler materials was very expensive and the production rate was very low. More recently, an attempt has been made by Pramanick et al. [7] to use specially designed matching SMAW electrode. The results showed that homogenous microstructure in the weld metal region can be obtained, together with excellent material properties through strict control of weld composition. However, as with the hardfaced interlayering technique, the production rate

✉ Zengxi Pan
zengxi@uow.edu.au

[1] School of Mechanical, Materials, Mechatronic and Biomedical Engineering, University of Wollongong, Northfield Avenue, Wollongong, NSW 2522, Australia

[2] Defence Materials Technology Centre, 24 Wakefield Street, Hawthorn, VIC 3122, Australia

remained very low since multiple weld passes were needed to fill the prepared weld, and the production of the specially designed electrode was very complex and time-consuming. In order to achieve high efficiency, low cost and improved material properties, the feasibility of using friction stir welding to join high strength Q&T steel was investigated by El-Batahgy et al. [12]. Although excellent mechanical properties were achieved together with high efficiency, the plate thickness was limited to 2 mm due to the poor fatigue resistance and durability of the friction stir tool. This means that FSW is not currently suitable for welding such steel with medium thickness.

Keyhole tungsten inert gas welding, also known as K-TIG, is a novel keyhole mode welding process which relies on high welding current and heavy arc pressure to displace the molten pool aside to form keyholing process, as opposed to high power density welding processes which rely on recoil pressure to open the keyhole. Compared with high power density laser-based welding or electron beam welding process, K-TIG is significantly lower cost and easier to operate, and has much better gap bridging capability. Due to single pass full penetration capability of the keyhole process, it has been widely used to weld medium thickness materials, such as 6 mm pure zirconium [13], 10 mm austenitic stainless steel [14] and 10.5 mm duplex stainless steel [15]. Lathabai et al. [16] conducted a study in which 12.7 mm pure titanium was welded by both conventional multipass TIG welding as well as K-TIG welding process in order to make a comparison between them. It was shown that the mechanical properties of K-TIG welded joint were similar to that produced by conventional TIG welding. More importantly, single pass full penetration was achieved without edge preparation at a speed of 250 mm/min for K-TIG welding process, as opposed to six passes welding with double V edge preparation at a speed of 150 mm/min for each pass in conventional TIG welding, which demonstrated the much higher efficiency of K-TIG than conventional multipass arc welding processes. However, as K-TIG welding relies on high welding current to increase arc pressure to achieve full penetration in medium thickness materials, the heat input used is relatively high, which may lead to undesired microstructure in the weld metal and deteriorate the weld properties. This was demonstrated by Fei et al. [17] who applied K-TIG to join medium thickness armour grade quenched and tempered steel in order to increase the productivity. It was found in their study that although the mechanical properties of joint produced by K-TIG are better than the weld produced by conventional welding with under-matching filler material, the hardness in the K-TIG weld metal region was still much lower than the base metal due to the formation of bainitic microstructure in the weld metal region, which resulted in unsatisfactory ballistic performance. In addition, the lower hardness in the weld metal also decreased the joint efficiency to some extent, making it less than that produced by using matching filler in conventional fusion arc welding processes (more than 70%). Considering that K-TIG welding process could lead to significant cost savings and higher production rates, if the microstructure in the weld metal region of K-TIG welded joint can be modified, then both excellent material properties and high production efficiency could be achieved. Recently, Fang et al. [18] tried to introduce ultrahigh frequency pulse in K-TIG welding to modify the weld microstructure. Although grain size was refined, the change in microstructure and improvement on mechanical properties was very limited. Also, the ultrahigh frequency pulse is harmful to health. Therefore, other methods need to be developed to fulfill the full potential of K-TIG welding process and the potential way is to apply filler material. As in keyhole TIG welding process, the weld pool distribution under the arc is different from conventional fusion welding process due to the formation of keyhole channel, the introduction of filler metal may complicate the interaction between welding arc and the weld pool. Whether the introduction of filler material is feasible in K-TIG welding should be evaluated. More importantly, whether the introduction of filler materials can produce homogeneous microstructure and improved material properties should also be determined.

It is known that chromium and nickel both possess a high contributing coefficient (1/5 and 1/15, respectively) in the formula of carbon equivalent, which is normally applied during welding and is related to the critical cooling time for the formation of full martensitic structure [19]. Therefore, this study will investigate the effectiveness of introducing ER308 austenitic filler metal into the K-TIG welding process for modifying the weld metal microstructure of a medium thickness high hardness armour (HHA) joint. In the following session, the material and fabrication methods will be described. The metal transfer behaviour will be analysed and a detailed characterization of the weld joint will be presented, including microstructure, hardness, tensile properties and impact toughness.

2 Materials and methods

The materials and filler wire used in this study were 6.2 mm HHA plates and ER308 austenitic filler materials, respectively, with their chemical composition listed in Table 1. Single pass full penetration was achieved using a welding machine manufactured by Keyhole TIG Limited with capacity of up to 1000 A. Bead-on-plate welding experiments were conducted on all the eight tests, while close square butt joint welding experiments were also conducted on both test 1 and 3 samples for undertaking tensile and impact tests. The dimension of bead-on-plate test plate was 250 mm × 140 mm, while two plates, each with dimension of 250 mm × 140 mm, were used to conduct close square butt welding experiments. For close

Table 1 Chemical composition of HHA and ER308 filler (wt.-%)

	C	Si	Mn	P	S	Ni	Cr	Fe
HHA	0.27	0.3	0.3	0.014	0.0025	0.19	1.05	Bal.
ER308	0.04	0.3	1.8	0.009	0.009	9.5	20	Bal.

square butt joint, the edges of the two plates were in close contact with each other with no joint gap. The square edges were milled till 90°. The surface of the plates and square edges were ground and cleaned by acetone before welding. As reported by Jarvis and Ahmed [20], wider electrode diameter and smaller electrode tip angle can induce a more constricted arc and reduce the threshold current to achieve full penetration. Therefore, 6.4 mm diameter electrode with 45° tip angle was chosen based on the reference data in the literature. The most appropriate arc length during K-TIG welding was found by Feng [14] to be 2.5 mm. After the electrode geometry and arc length were properly identified, the most important welding parameters controlling the weld formation, such as welding current and travel speed, were adjusted by control variable method. Then, matching current and travel speed values producing full penetration with good bead appearance were identified and selected. In order to observe the free slight transfer mode, 8 mm arc length was also applied. Detailed welding parameters are shown in Tables 2 and 3. During the welding process, filler wire was fed into the weld pool from the leading side using a generic wire feeder. A high frame-rate digital camera was placed perpendicular to the travel direction to capture the metal transfer behaviour. The frame rate was set at 1 and 3 KHz for tests 2 to 4 and tests 5 to 8, respectively. The worktable was moved at the preset speed while the welding torch was kept stationary to simplify observation of welding process. The schematic of the welding system is shown in Fig. 1. The plates were preheated at 150 °C prior to welding in order to reduce the risk of hydrogen-assisted cold cracking.

After welding, the joints were sectioned and polished for both macro- and micro characterization by Leica M205A stereomicroscope as well as Nikon Eclipse LV100DNA optical microscope and JEOL JSM-7001F field emission gun SEM, respectively. Two per cent nital was used as an etchant to reveal the microstructure. EDS point analysis was conducted on the welded joint at three different locations in order to calculate the dilution rate of weld metal. Vickers microhardness was carried out along the through-thickness direction as well as the transverse direction across the weld at an interval of 0.5 mm with a load of 1 kg and 10 s dwell time using Struers DuraScan-70 automatic hardness tester. The tensile samples and impact toughness samples were cut in the direction perpendicular to the welding direction, with their dimension shown in Fig. 2. The tensile tests were undertaken as per

Table 2 Fixed welding parameters

Process parameters	Details
Current, A	480
Travel speed, mm/min	350
Shielding gas	Pure argon
Shielding gas flow rate, L/min	25
Wire feeding angle (degree)	40
Filler wire	ER308
Wire diameter (mm)	1.2
Operation mode	DCEN

ASTM E8 standard. The tensile tests were undertaken at room temperature at a constant strain rate of 1 mm/min^{-1} and a 50-mm gauge length using an Instron 8800 universal testing machine. An extensometer with a nominal gauge length of 50 mm was used to measure percentage elongation. Charpy V-notch impact tests were carried out as per ASTM E23 standard. The notch was made in the middle of weld metal for test 1 and test 3 samples. The impact tests were performed at room temperature. For tensile and impact tests, three samples were tested in each case and an average values were taken into consideration from three samples in order to test the repeatability of the results. The fracture surface of the welded joint was observed by JEOL JSM-6490 SEM.

3 Results and discussion

3.1 Metal transfer behaviour

For cold-wire TIG welding, the metal transfer modes can be divided into four types, namely intermittent wire melting, uninterrupted bridging transfer, interrupted bridging transfer and free flight transfer [21]. As shown in Fig. 1, in the K-TIG process, the weld pool in front of the keyhole channel is very thin due to its keyhole nature, as demonstrated by Li et al. [22], which makes it difficult in practice to accurately feed the wire towards the weld pool to achieve uninterrupted bridging transfer. In addition, the dilution rate will be significantly affected with intermittent wire melting. Therefore, the other transfer modes become the typical practice in K-TIG welding.

The metal transfer behaviour of the tests with 2.5 mm arc length is shown in Fig. 2. All the three tests with 2.5 mm arc length and applied filler materials (tests 2 to 5) show typical interrupted bridging transfer mode, which is very similar to short circuit transfer mode in the GMAW process. Once the droplet size reaches a critical level, it touches the weld pool and transfers into the weld pool through surface tension effects and the wire is then separated from the weld pool. The metal

Table 3 Variable process parameters for all test sample

Test number	Wire feed speed (cm/min)	Arc length (mm)	Joint type
1	0	2.5	Bead-on-plate/square butt
2	36	2.5	Bead-on-plate
3	85	2.5	Bead-on-plate/square butt
4	158	2.5	Bead-on-plate
5	300	2.5	Bead-on-plate
6	158	8	Bead-on-plate
7	220	8	Bead-on-plate
8	300	8	Bead-on-plate

transfer period ranges from 216 ms in test 3 to 33.5 ms in test 5 as the wire feed speed (WFS) increases due to increased melting speed as the wire moves closer to arc column. The droplet in test 5 sees evident growth before it touches the weld pool since the distance between the droplet and the weld pool increases when the wire goes further into the keyhole channel. Therefore, a larger droplet is required to make contact with the weld pool to finish the transfer. It is noted that the WFS achievable in K-TIG is much faster than that in plasma arc welding (less than 150 cm/min with 0.9 diameter filler wire [23]), which offers a greater scope for microstructure modification.

In tests 6–8, the arc length is increased to 8 mm. As can be seen from Fig. 3a, b, the droplet grows slowly and it is not possible for the droplet to touch the weld pool for the long arc length. Once the droplet grows large enough, its weight overcomes the surface tension force that suspends it from the wire and it drops onto the weld pool through globular transfer which is the same as that seen in the GMAW process. The transfer period is longer than that of interrupted bridging transfer. For test 8 with 300 cm/min WFS, the wire tip is closer to the arc column and is partially melted due to the very high arc temperature, resulting in a quasi-tapered shape of the electrode end, as shown in Fig. 3c. It is observed that the transfer frequency becomes extremely high (less than 2.33 ms) by tracking the droplet highlighted by red arrow. According to static force balance theory proposed by Waszink and Graat et al. [24], the resultant detaching force on a droplet can be expressed as follows:

$$F_d = F_g + F_a + F_{em} - F_v - F_\sigma \quad (1)$$

Where F_g, F_{em}, F_v, F_a, and F_σ represent gravity, electromagnetic force, vapour jet force, plasma drag force, and surface tension, respectively. As the tapered electrode end induces a dramatic reduction in F_σ, the mass dependent F_g is also much reduced. Therefore, the droplet would be detached at a much smaller size and the transfer frequency was considerably increased accordingly. This transfer mode is very similar to streaming transfer mode in GMAW.

Considering that in the free flight transfer mode, the transfer frequency is much slower, which would allow the liquid droplet to be exposed to high temperature for longer time and thus lead to loss of alloy element. Also, free flight transfer mode tends to generate spatter defect. Therefore, interrupted bridging transfer mode is considered to be the preferential way to feed the wire in K-TIG welding process. It is worth mentioning that for test 2 with WFS as low as 36 cm/min, repelled globular droplet was experienced when wire was fed from the leading side of the weld pool. When the WFS is very low, the wire tip melts at the arc edge region, and the forces of F_a and F_{em} are very small, so the vapour jet force acts as a dominant repulsive force to prevent the droplet from being detached, leading to wobbling of the droplet and irregular transfer behaviour. For this reason, the wire was fed into the weld pool from the trailing side of the weld at this low value of WFS.

3.2 Macrostructure and dilution

Samples from tests 1–4 were chosen for further characterization, with macrograph shown in Fig. 4a–d. Single pass full penetration was achieved without any visible defects. The weld metal width (W_f), heat-affected zone width (W_h) and front side reinforcement (h) were measured based on the schematic illustrated in Fig. 4e. It is shown in Fig. 4f that the introduction of filler materials leads to increased h from 0.36 to 1.1 mm. In addition, both W_f and W_h experience a clearly decreasing trend when filler wire is introduced to the weld pool, especially when the wire is fed from the leading side. This is due to the fact that increased metal vapour emanating from the molten wire increases the radiation loss because of the difference in net radiation coefficient between argon and metal vapour, which allows the constriction of arc isotherms to occur [25, 26].

EDS X-ray analysis was carried out in three zones in the weld metal region, namely the upper, middle and lower regions, as indicated by blue dots in Fig. 4e. Since the ER308 filler material is rich in chromium and nickel, the content of these two elements is used to calculate the dilution rate. The dilution in this study is defined as the weight percentage of filler deposited in the weld metal. The way in which the

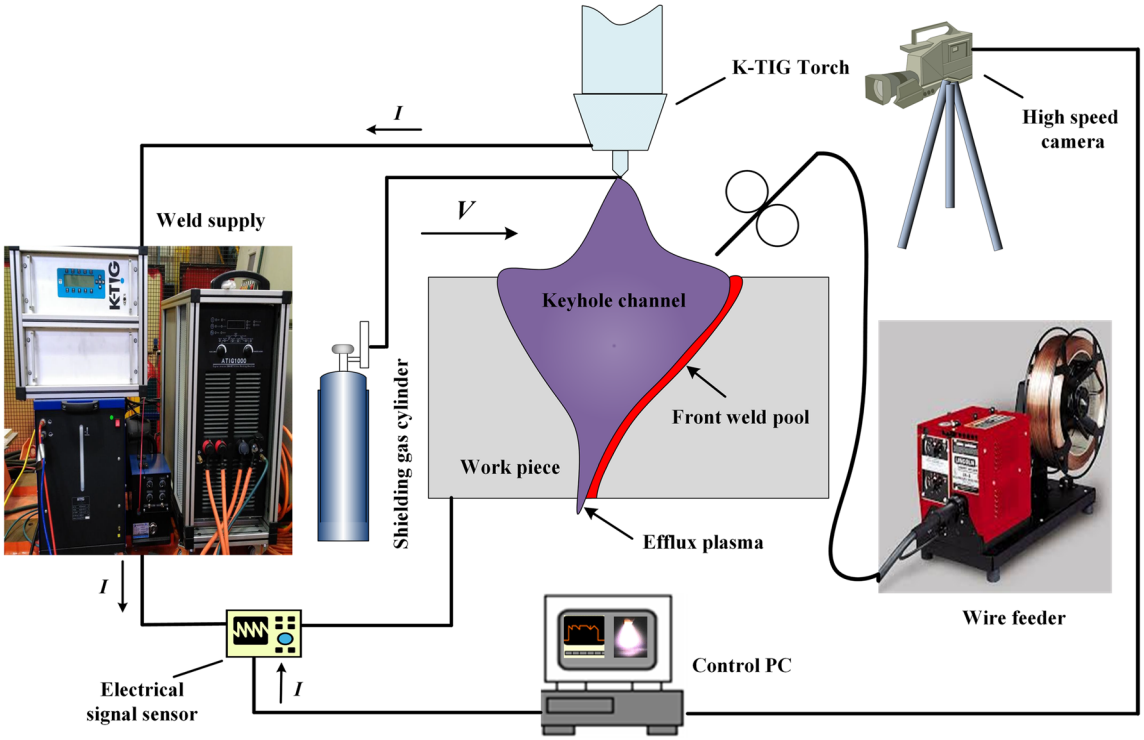

Fig. 1 Schematic of K-TIG welding system with filler wire

dilution rate is calculated is shown in Eq. 2 and Eq. 3 based on the concentration of chromium and nickel in base metal and weld metal.

$$20d + 1.05(1-d) = Cr_w \quad (2)$$

$$9.5d + 0.19(1-d) = Ni_w \quad (3)$$

Where d is the dilution rate; Cr_w and Ni_w represent the average concentration of chromium and nickel in the weld metal, respectively. It can be seen that the dilution rate d can be obtained by directly solving a linear equation. The dilution rates calculated from chromium and nickel are very close, with the average value of them taken into consideration and

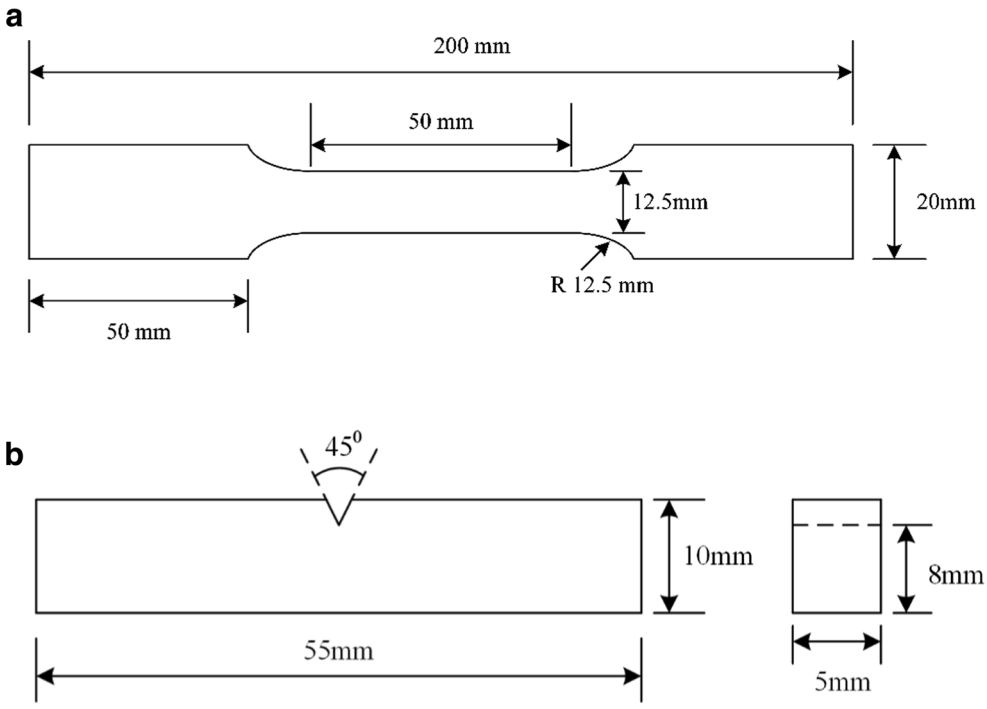

Fig. 2 Test sample dimension. **a** Tensile test sample. **b** Charpy impact toughness test sample

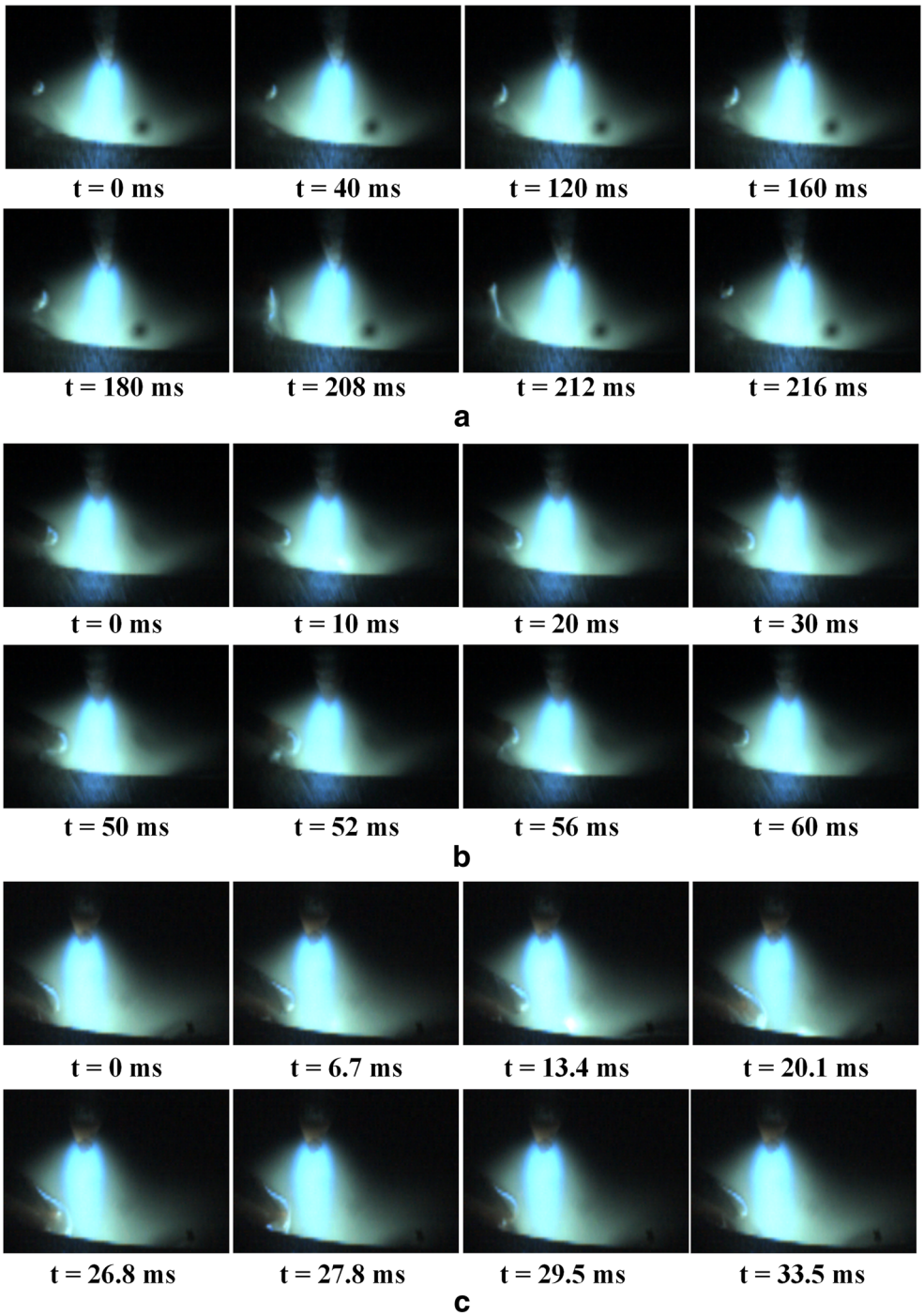

Fig. 3 Metal transfer behaviour with different WFS at arc length of 2.5 mm. **a** Test 3 (WFS = 85 cm/min). **b** Test 4 (WFS = 158 cm/min). **c** Test 5 (WFS = 300 cm/min)

listed in Table 4. The average content of chromium and nickel increases from 1.05 and 0.19% in the base metal to a maximum of 3.3 and 1.3% in the weld metal. The dilution rate is 2.74%, 6.68 and 11.88% for 36 cm/min, 85 cm/min and 158 cm/min WFS, respectively. The chemical composition in the weld varies little along the through-thickness direction, indicating a homogenous dilution in the entire weld metal region.

3.3 Microstructure

The microstructures of base metal and the weld metal region of four test samples are shown in Figs. 5 and 6. The base metal consists of tempered martensite resulting from typical quenching and tempering heat treatment, as shown in Fig. 6a. In the as-welded condition of test 1 sample, as depicted in Fig. 6b, the microstructure of weld metal consists

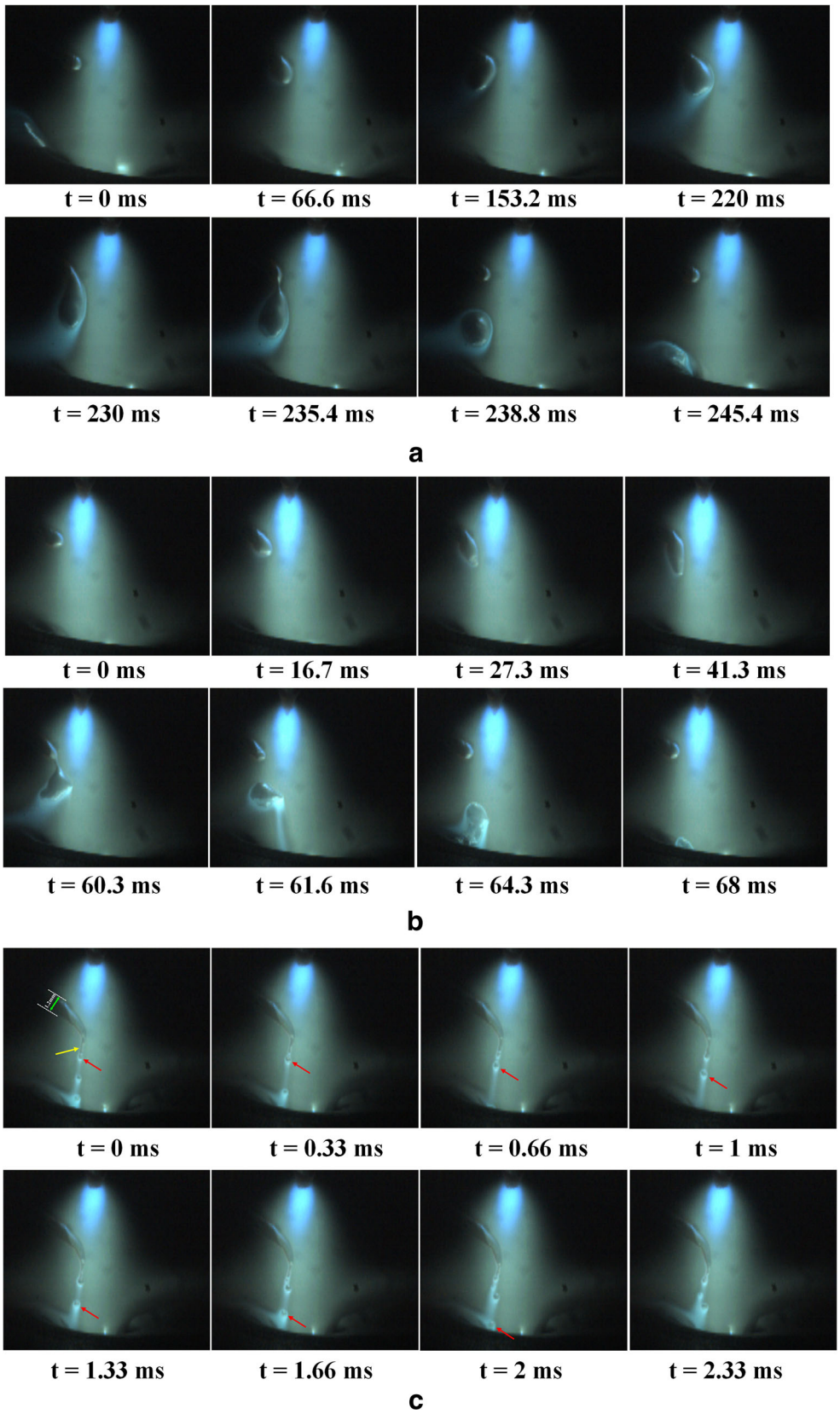

Fig. 4 Metal transfer behaviour with different WFD at arc length of 8 mm. **a** Test 6 (WFS = 158 cm/min). **b** Test 7 (WFS = 220 cm/min). **c** Test 8 (WFS = 300 cm/min)

Table 4 Chemical analysis of weld metal

WFS (cm/min)	Weld chemical composition (wt.-%)								Dilution rate (%)
	Upper		Middle		Lower		Average		
	Cr	Ni	Cr	Ni	Cr	Ni	Cr	Ni	
36	1.49	0.45	1.62	0.47	1.63	0.41	1.58	0.44	2.74
85	2.32	0.81	2.43	0.81	2.27	0.78	2.34	0.8	6.68
158	3.38	1.4	3.53	1.29	3	1.2	3.3	1.3	11.88

predominantly of banitic microstructure. With 2.74% dilution, the microstructure changes from bainite to a mixture of bainite and martensite as depicted in Fig. 6c. Once the dilution rate is increased to 6.68%, the microstructure becomes fully martensitic (Fig. 6d). A further increase in dilution beyond 6.68% has little influence on the microstructure as shown in Fig. 6e. High magnification SEM image was also taken at weld metal region of test 1 and test 3 samples for detailed observation. As shown in Fig. 6f, the microstructure of weld metal in test 1 sample consists of upper bainite with aligned carbides in between bainitic sheaves as well as granular bainite which is a combination of irregular-shaped ferrite and dispersed blocky or elongated RA/martensite constituent. The microstructure of weld metal in test 3 shows typical morphology of lath martensite, as depicted in Fig. 6g, which is consistent with the results from optical microscope.

It is known that the addition of chromium and nickel can change the carbon equivalent and influence the continuous cooling curve (CCT) diagram of investigated armour steel by changing the interaction point of cooling curve of weld metal with phase transformation curve of various phases, say ferrite, bainite and martenite and retarding high temperature phase transformation. Thus, it can be inferred that for the investigated armour steel, the cooling curve of weld metal interacts with both bainite start and finish line, all the undercooled austenite transforms into bainite. With 2.74% dilution from austenitic filler, the bainite transformation curve moves rightward, which allows the cooling curve of weld metal to interact only with bainite start line. Thus, the transformation of austenite into bainite is incomplete, with the remaining austenite transforming into martensite. Once the dilution reaches 6.68% or beyond, the bainite transformation curves move further rightward, with the results being that the cooling curve of weld metal does not interact with bainite start line and enters the martensite transformation region directly, leading to complete transformation from austenite to martensite.

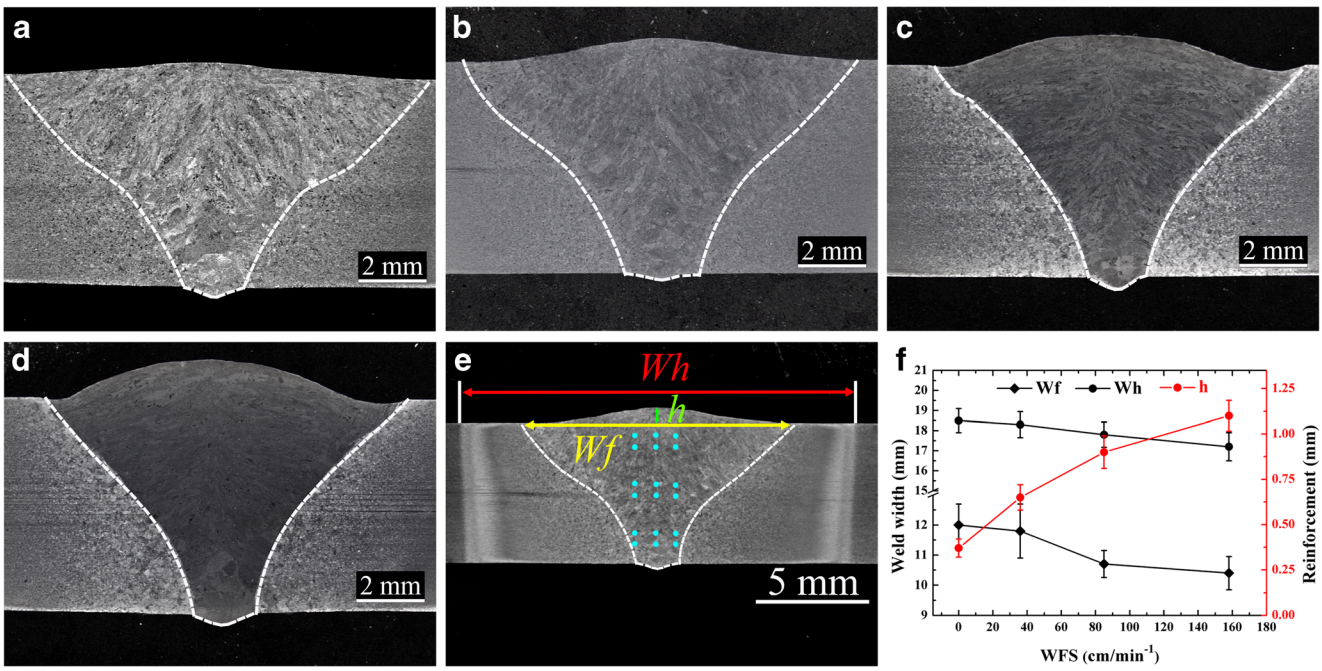

Fig. 5 Macrograph of K-TIG welded joint with and without filler wire **a** weld without filler; **b** WFS = 36 cm/min; **c** WFS = 85 cm/min; **d** WFS = 158 cm/min; **e** schematic of fusion zone geometry and EDS test position; and **f** weld geometry variation trend

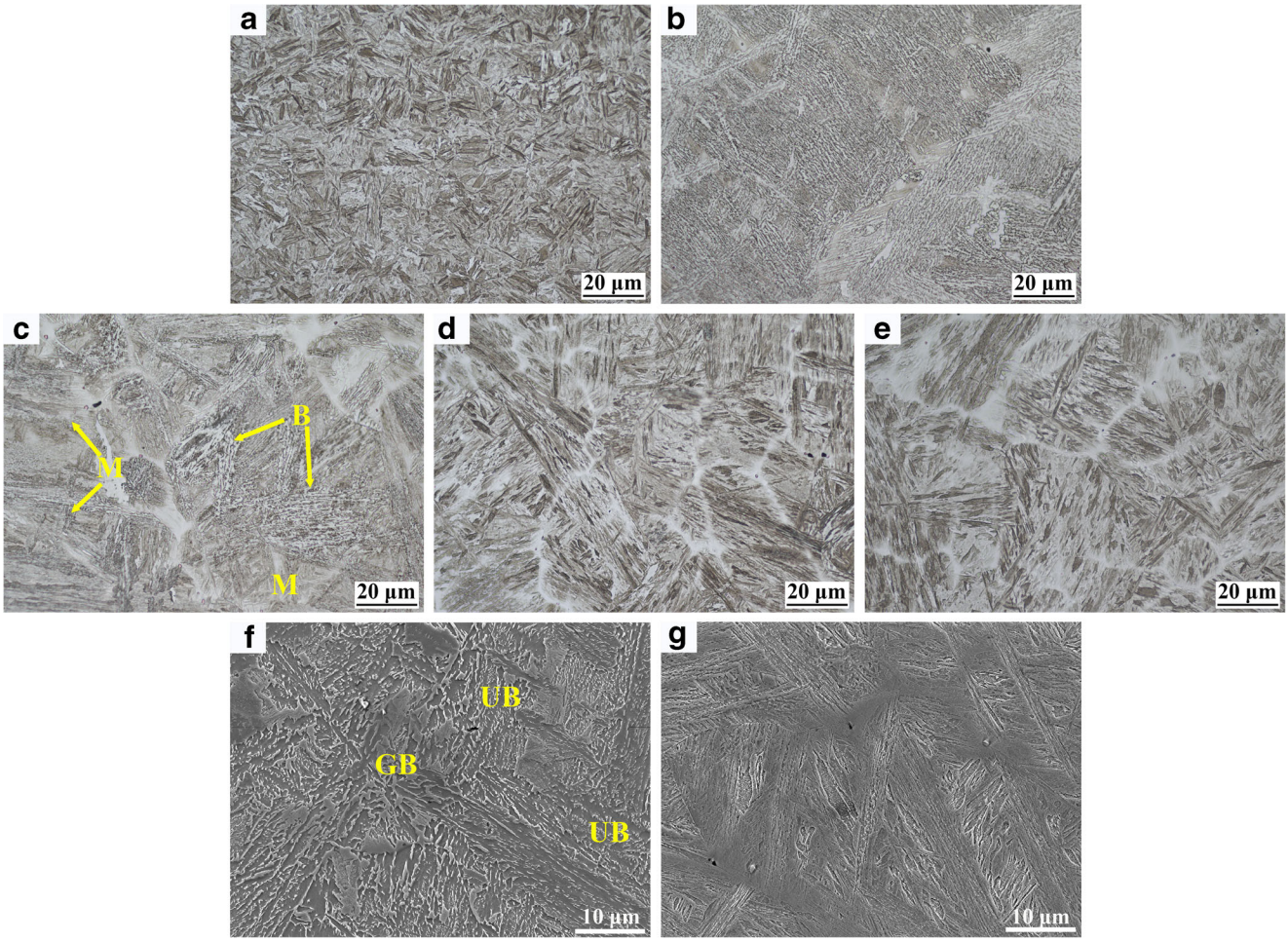

Fig. 6 Microstructure of base metal and weld with and without filler materials. **a** Base metal. **b** Weld metal without filler. **c** Weld metal with 2.74% dilution. **d** Weld metal with 6.68% dilution. **e** Weld metal with 11.88% dilution. **f** High magnification SEM of (**b**). **g** High magnification SEM of (**d**) (B: bainite, M: martensite, GB: granular bainite, UB: upper bainite)

The microstructure evolution across the weld is shown in Fig. 8. The heat-affected zone (HAZ) can be divided into four subzones, namely coarse grain HAZ, fine grain HAZ, intercritical HAZ and over-tempered region. In the coarse grain HAZ, which refers to the region heated to a high temperature during welding thermal cycle, large amount of bainite and small amount of martensite is formed, as shown in Fig. 7a. Due to the rapid grain growth in the high temperature region, the coarse austenite retransforms into coarse martensite and bainite structure. In fine grain HAZ, except for the much smaller grain size, the martenite becomes dominant microstructure, with only small fraction of bainite formed in this region, as indicated in Fig. 7b. It is because in the fine grain HAZ, the temperature experienced is lower than coarse grain HAZ, which leads to faster cooling rate and thus favours the formation of martensite. In intercritical HAZ, which is heated to dual phase $\alpha + \gamma$ region, part of the martensite in the base metal transform to ferrite through recrystallization mechanism, with the remaining martensite transforms into austenite. The reformed austenite would transform to martensite and bainite upon cooling, resulting in the mixture of martensite, bainite and polygonal ferrite in this region, as depicted in Fig. 7c. The microstructure of over-tempered (OT) region adjacent to intercritical HAZ is shown in Fig. 7d and is composed of heavily tempered martensite. Compared with base metal microstructure as shown in Fig. 7e, larger amount of carbide particles precipitated both along prior austenite grain boundaries and inside grains, which is a result of high temperature tempering experienced in this region.

3.4 Hardness

The hardness distribution along the through-thickness direction and the average hardness are illustrated in Fig. 8. The average hardness increases from 340 to 392 Hv as the microstructure changes from bainite to the mixture of martensite and bainite with 2.74% dilution. When the dilution reaches 6.68%, the hardness increases considerably to 528 Hv due to the formation of a fully martensitic microstructure. Further increase in dilution rate imposes little effect on the increase in hardness

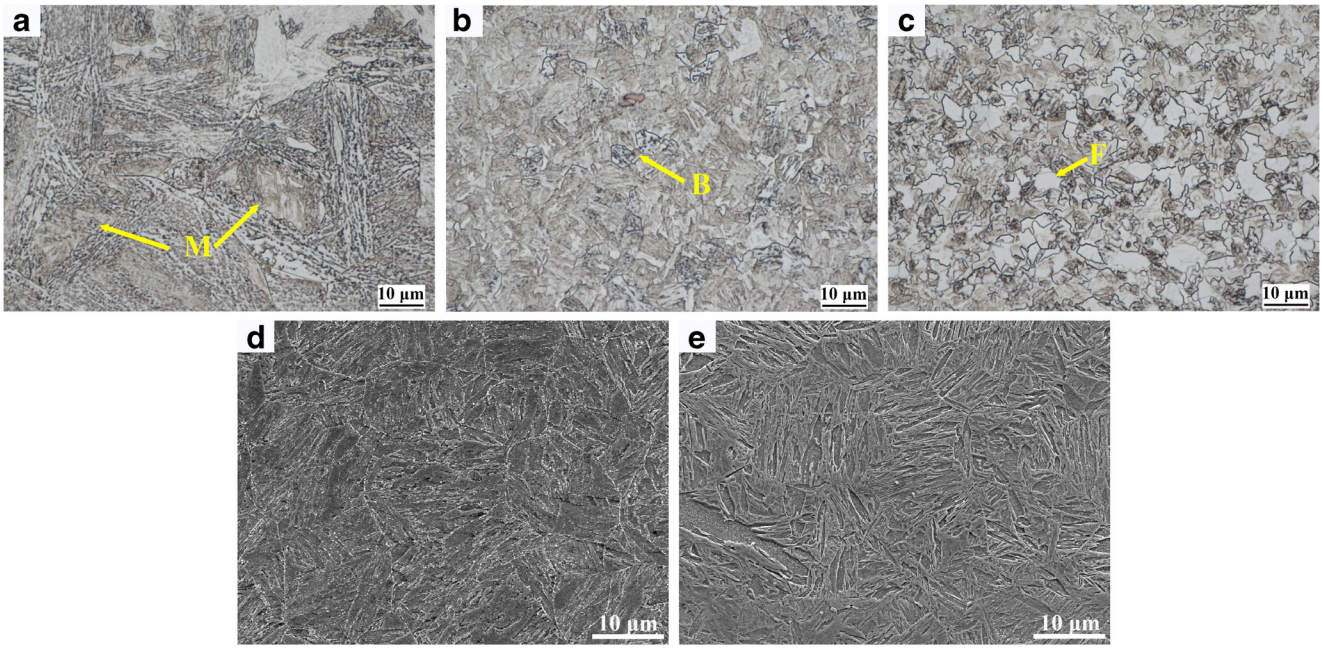

Fig. 7 Microstructure of HAZ. **a** Coarse grain HAZ. **b** Fine grain HAZ. **c** Intercritical HAZ. **d** Over-tempered region. **e** Base metal; (F: ferrite)

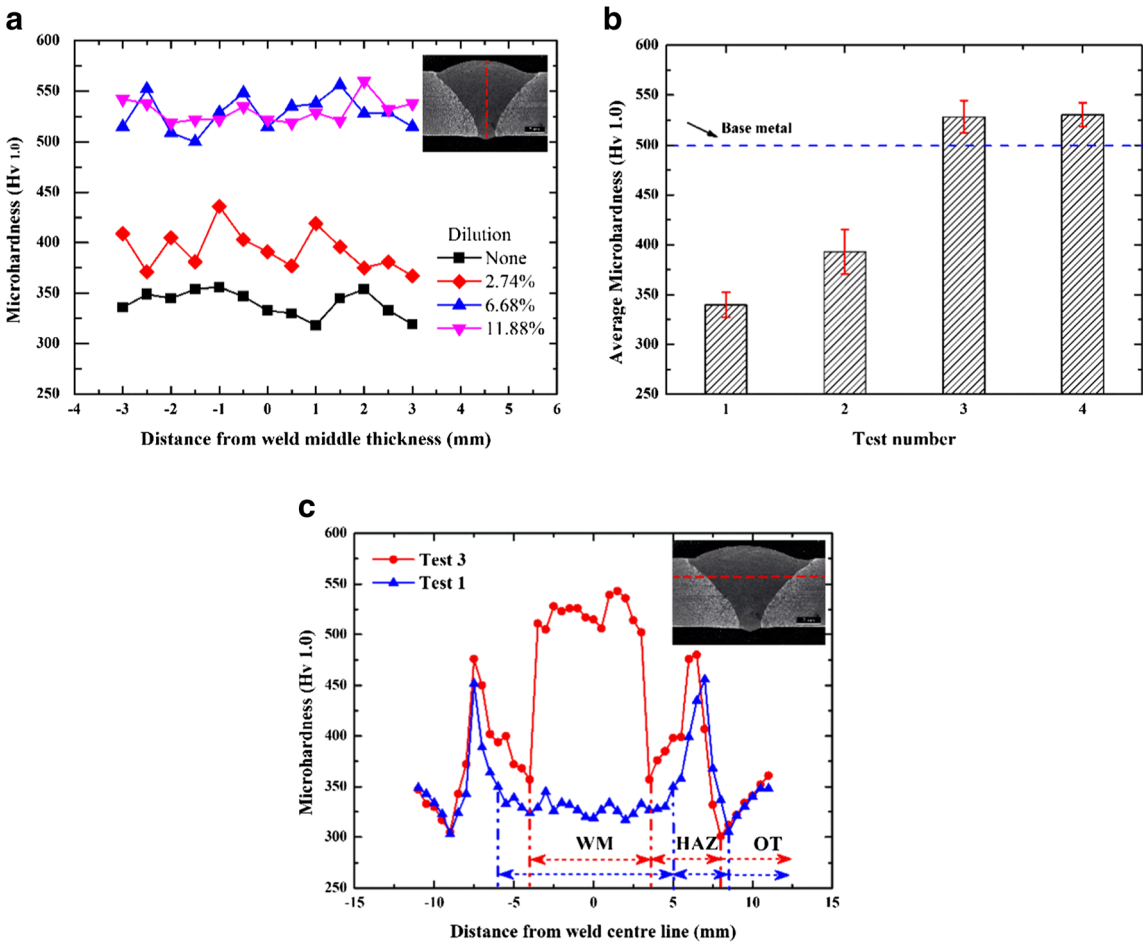

Fig. 8 Hardness in weld metal with different dilution. **a** Hardness distribution along through-thickness direction. **b** Average hardness. **c** Hardness distribution across weld

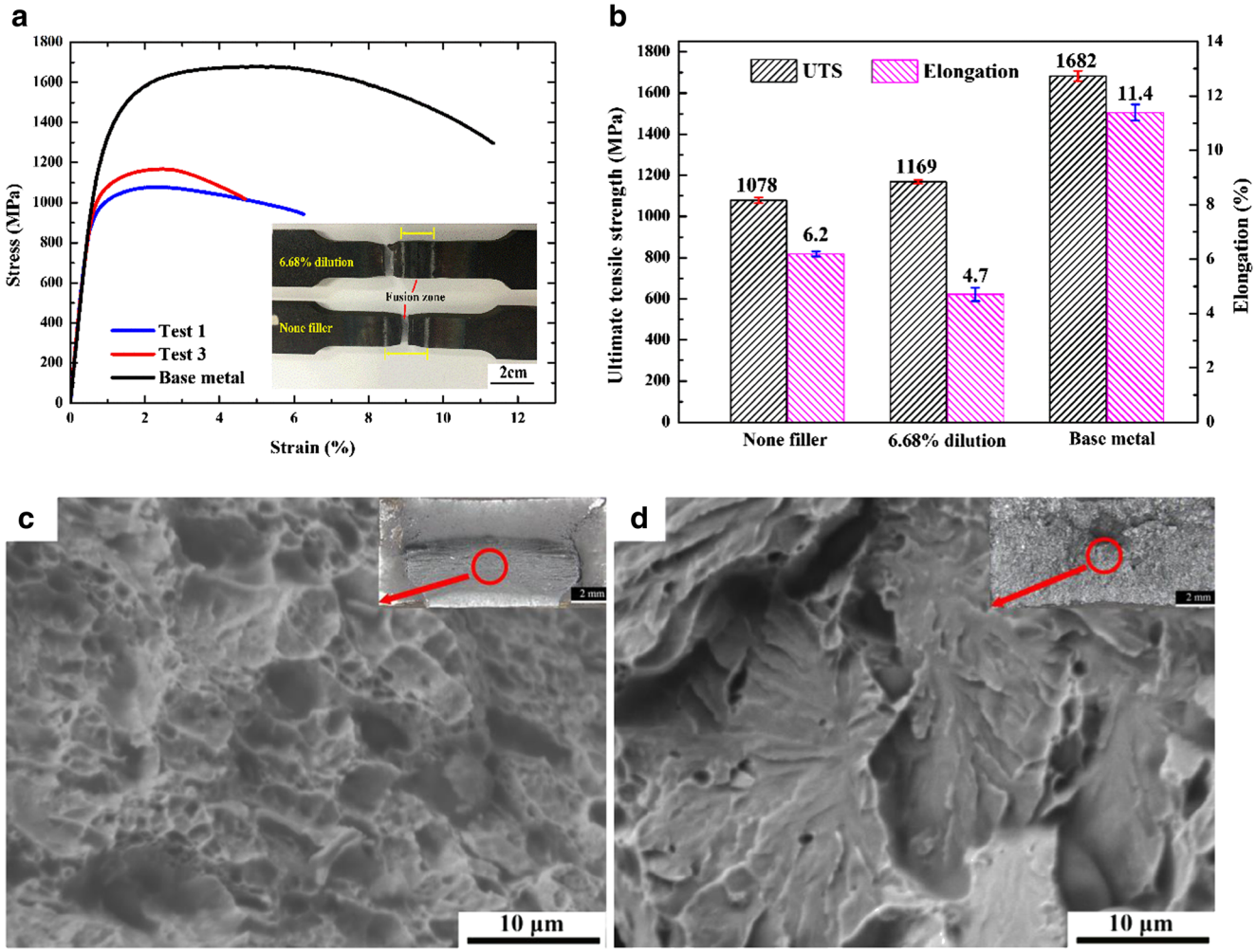

Fig. 9 Tensile properties of welded joint. **a** Tensile curve. **b** Results of tensile test. **c**, **d** Images of fracture surface of test 3 and test 1 joints, respectively

due to the similar microstructure to the weld with 6.68% dilution, with the hardness being 530 Hv with 11.88% dilution. It can be seen that the hardness of the weld with 2.74% dilution experiences the largest hardness fluctuation, which might indicate that it is the critical point for the transformation from bainite to martensite. It is also found that 6.68% dilution is optimal from the perspective of both increased hardness and cost-effectiveness. The hardness in the weld metal region (530 Hv) is much higher than the weld produced with under-matching filler and is at the same level as the weld deposited by specially designed matching filler in [7] with as little as 6.68% dilution from austenitic filler compared with the weld consisting of almost 100% of specially designed electrode material. The hardness distribution across the weld is shown in Fig. 8c. The hardness of the HAZ increases from around 360–400 Hv in the coarse grain HAZ to 450–480 A in the fine grain HAZ, followed by the decrease in hardness to the lowest point as it moves through intercritical HAZ to the interaction point between intercritical HAZ and subcritical HAZ. Then, the hardness would increase gradually in the subcritical HAZ until it reaches the hardness of base metal (500 Hv). The hardness distribution is consistent with the microstructure change across the weld.

3.5 Tensile properties

Figure 9a shows the tensile curve of test 1 (no filler) and test 3 (6.68% dilution) joints. All the three test 1 tensile samples fractured in the weld metal region while all the three test 3 tensile samples fractured in subcritical HAZ. It can be seen from Fig. 7b that the UTS and joint efficiency for test 1 and test 3 joint are 1078 MPa and 64.2%, and 1169 MPa and 70%, respectively. The difference in the test results can be ascribed to the formation of much harder and stronger maternsitic microstructure in the weld metal region. As can be seen from the hardness distribution in Fig. 8c, the weakest region of HAZ is located in over-tempered region adjacent to intercritical HAZ where the average hardness is around 300–330 Hv. For the test 1 sample without filler dilution, the average hardness in the weld is comparable to that in the weakest region. However,

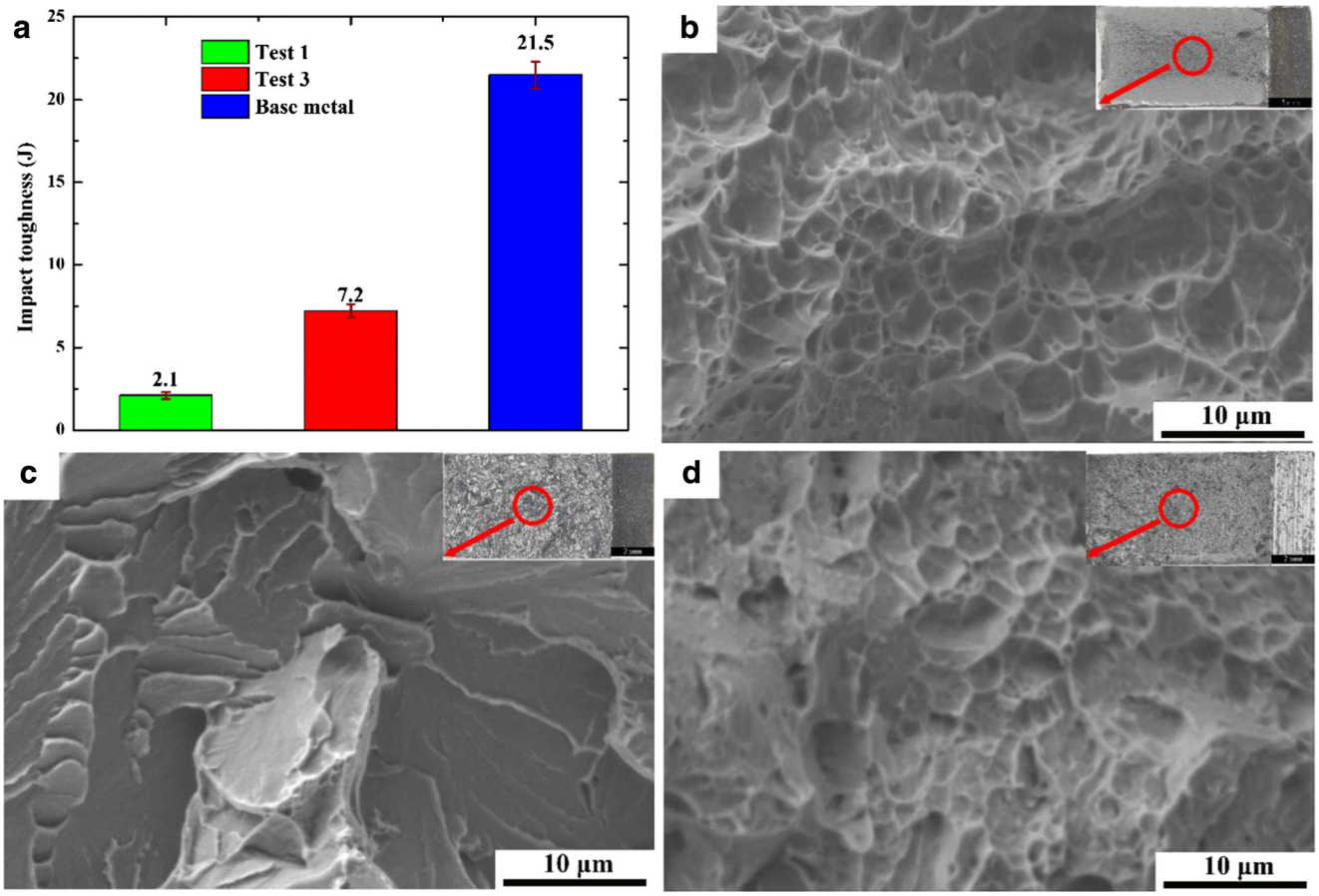

Fig. 10 Charpy impact toughness. **a** Impact results. **b**, **c** and **d** Images of fracture surface of base metal, test 1 joint and test 3 joint, respectively

due to the very small size (less than 1 mm) in the weakest region compared with the weld metal region, the localized strain tends to occur in the weld metal, leading to the final fracture at this region. When filler wire is introduced, as in test 3 sample, the weld hardness is increased to 530 Hv. Thus, the weakest region becomes longer (more than 3 mm) compared with the second weakest region in coarse grain HAZ. The localized strain then transfers from the weld metal region to the weakest region across the weld, leading to the change in fracture location from weld metal to the over-tempered region. The elongation of the test 3 joint is 4.7% which is slightly lower than test 1 joint. This is attributed primarily to the increased strength mismatch associated with higher hardness in weld metal than base metal. A similar phenomenon has also been reported in [12] during friction stir welding. As with the hardness improvement, the joint efficiency of test 3 joint (70%) is much higher than joints produced by conventional welding processes (47 and 64% for austenitic and ferritic filler, respectively [27]).

The fracture surfaces of these two joints are shown in Fig. 7c, d. The macrographs of the fracture surfaces, inserted in the upper right of the figures, show that the fracture surface of test 3 joint is composed solely of fibrous zone and shear lip zone, whereas that of test 1 joint consists predominantly of radial zone. The high magnification SEM images of fracture surfaces in the areas highlighted by red circles show that test 3 joint contains dimples typical of ductile fracture, whereas test 1 joint exhibits typical cleavage fracture with river pattern characteristics. The large difference in fracture mode is ascribed to the difference in microstructure in the fracture location, which is heavily tempered martensitic microstructure in test 3 sample and bainitic microstructure in the test 1 sample. It is known that the tempered martensite possess good toughness due to the large fraction of high angle grain boundary as well as the low stress concentration associated with tempering process, which provides great resistance to cleavage fracture and results in a ductile fracture mode. For the banitic microstructure in test 1 weld region, the brittle M/A constituent and low fraction of high angle grain boundary associated with upper bainite and granular bainite decrease both crack initiation and propagation energy, which will be further discussed in the following section.

3.6 Impact toughness

The impact toughness results of test 1 sample, test 3 sample and base metal are 2.1 J, 7.2 J and 21.5 J, respectively, as

shown in Fig. 10a. This is consistent with the macrographs of the fracture surfaces inserted in the upper right of Fig. 10b–d. The shear lip on the fracture surface of base metal is thick while that on the fracture surface of test 3 sample is relatively thin and the fracture surface is flatter. When it comes to test 1 sample, the fracture surface consists predominantly of bright radial zone similar to that in tensile sample, which implies rapid crack propagation and typical cleavage fracture mode. High magnification of fracture surface shows that the base metal and test 3 sample are composed of large amount of dimples whereas test 1 sample consists of cleavage facet and step. It is worth noting that the dimples on the fracture surface of base metal are larger and deeper than test 3 sample, indicating more absorbed energy and a better impact toughness.

Due to the larger prior austenite grain size and inherited substructure in the weld metal of test 3 sample compared with base metal, the effective grain size, which refers to the total length of the grain boundaries with misorientation more than 15° per unit area, will be decreased, which leads to less crack deflection and arrest, and deteriorates the toughness in test 3 sample. The increased toughness of test 3 sample compared with test 1 sample is related to the brittle M/A constituent and the fraction of high angle grain boundaries. It was reported that large M/A constituent, as the ones shown in Fig. 6f, would reduce the critical fracture stress based on the classical Griffith theory and thus make it easier for the debonding of M/A constituents from surrounding bainitic matrix [28, 29], leading to reduced crack initiation energy. Once cracks initiate, the subsequent propagation is governed by high angle misorientation angle which is regarded as the sole effective obstacle for crack propagation. As the lath martensite is known to have larger fraction of high angle grain boundaries compared with granular bainite and upper bainite [28, 30], more crack deflection and arrest will be induced, which would consume more energy and result in increased impact toughness. Furthermore, except for the lower fraction of high angle grain boundaries in bainitic microstructure, the high angle grain boundaries in coarse bainitic microstructure has been reported to have little effect on the deflection and arrest of cracks, and cleavage fracture mechanism of coarse bainite is controlled by crack initiation [29]. Therefore, rapid crack propagation would occur after initial crack forms, which is consistent with the fracture surface. These could probably explain the very poor toughness in test 1 sample. Future research will focus on the refinement of grain size in the weld metal region in order to further improve the toughness.

4 Conclusions

In summary, the use of austenitic filler material has been successfully introduced in K-TIG welding of 6.2 mm HHA plates. Single pass full penetration was achieved at a travel speed of 350 mm/min and wire feeding speed (WSF) up to 300 cm/min, providing a large space for microstructure modification. Both interrupted bridging and free flight metal transfer modes were practical in this process, with the interrupted bridging transfer being the preferential way to feed the wire. In the case of very slow WFS (36 cm/min), the wire needs to be fed into the weld pool from the trailing side of the weld pool in order to avoid repelled globular droplet. The use of filler material was found to be very effective in modifying microstructure and improving joint properties. As WFS was increased, the microstructure in the weld metal region changes from bainite to a mixture of martensite and bainite, and finally to a fully martensitic microstructure. The dilution rate of 6.68% was found to be the optimal level from the perspective of improved properties and cost-effectiveness. The hardness of weld metal and joint efficiency were increased from 340 to 530 Hv and from 64.2 to 70%, respectively. These results are much better than those achieved with conventional welding processes using under-matching filler, and are comparable to levels obtained by using specially designed matching filler, but with much increased production efficiency and cost saving. In addition, the toughness in the weld metal region was increased from 2.1 J in the weld produced without filler to 7.2 J in the weld with filler dilution. The increased hardness and toughness would also lead to much better ballistic performance. The introduction of filler material dramatically expands the capability of K-TIG welding process and also provides an efficient and innovative solution for producing high performance armour steel welded joints.

Acknowledgements This research has been conducted with the support of the Australian Government Research Training Program Scholarship. The authors acknowledge the support of the Defence Materials Technology Centre (DMTC), which was established and is supported by the Australian Government's Defence Future Capability Technology Centre (DFCTC) initiative. The JEOL JSM-7001F FEG-SEM was funded by the Australian Research Council (ARC)—Linkage, Infrastructure, Equipment and Facilities (LIEF) Grant LE0882613.

Compliance with ethical standards

Conflict of interest The authors declare that they have no conflict of interest.

References

1. Ade F (1991) Ballistic qualification of armor steel weldments. Weld J 70(9):53–58
2. Reddy GM, Mohandas T (1996) Ballistic performance of high-strengh low-alloy steel weldments. J Mater Process Tech 57(1–2): 23–30

3. Magudeeswaran G, Balasubramanian V, Balasubramanian T, Reddy GM (2008) Effect of welding consumables on tensile and impact properties of shielded metal arc welded high strength, quenched and tempered steel joints. Sci Technol Weld Joi 13(2): 97–105
4. Reddy GM, Mohandas T, Papukutty K (1998) Effect of welding process on the ballistic performance of high-strength low-alloy steel weldments. J Mater Process Tech 74(1–3):27–35
5. Mohandas T, Reddy GM, Kumar BS (1999) Heat-affected zone softening in high-strength low-alloy steels. J Mater Process Tech 88(1):284–294
6. Magudeeswaran G, Balasubramanian V, Reddy GM, Balasubramanian T (2008) Effect of welding processes and consumables on tensile and impact properties of high strength quenched and tempered steel joints. J Iron Steel Res Int 15(6):87–94
7. Pramanick AK, Das H, Reddy G, Ghosh M, Das G, Nandy S, Pal T (2016) Development and design of microstructure based coated electrode for ballistic performance of shielded metal arc welded armour steel joints. Mater Des 103:52–62
8. Reddy GM, Mohandas T, Papukutty K (1999) Enhancement of ballistic capabilities of soft welds through hardfacing. Int J Impact Eng 22(8):775–791
9. Balakrishnan M, Balasubramanian V, Reddy GM, Sivakumar K (2011) Effect of buttering and hardfacing on ballistic performance of shielded metal arc welded armour steel joints. Mater Des 32(2): 469–479
10. Balakrishnan M, Balasubramanian V, Reddy GM (2013) Effect of hardfaced interlayer thickness and low hydrogen ferritic capping on ballistic performance of shielded metal arc welded armour steel joints. J Iron Steel Res Int 20(12):82–91
11. Balakrishnan M, Balasubramanian V, Reddy GM (2013) Effect of hardfaced interlayer thickness on ballistic performance of armour steel welds. Mater Des 44:59–68
12. El-Batahgy A-M, Miura T, Ueji R, Fujii H (2016) Investigation into feasibility of FSW process for welding 1600 MPa quenched and tempered steel. Mater Sci Eng A 651:904–913
13. Lathabai S, Jarvis B, Barton K (2008) Keyhole gas tungsten arc welding of commercially pure zirconium. Sci Technol Weld Joi 13(6):573–581
14. Feng Y, Luo Z, Liu Z, Li Y, Luo Y, Huang Y (2015) Keyhole gas tungsten arc welding of AISI 316L stainless steel. Mater Des 85: 24–31
15. Cui S, Shi Y, Sun K, Gu S (2018) Microstructure evolution and mechanical properties of keyhole deep penetration TIG welds of S32101 duplex stainless steel. Mater Sci Eng A 709:214–222
16. Lathabai S, Jarvis B, Barton K (2001) Comparison of keyhole and conventional gas tungsten arc welds in commercially pure titanium. Mater Sci Eng A 299(1–2):81–93
17. Fei Z, Pan Z, Cuiuri D, Li H, Wu B, Ding D, Su L, Gazder AA (2018) Investigation into the viability of K-TIG for joining armour grade quenched and tempered steel. J Manuf Process 32:482–493
18. Fang Y, Liu Z, Cui S, Zhang Y, Qiu J, Luo Z (2017) Improving Q345 weld microstructure and mechanical properties with high frequency current arc in keyhole mode TIG welding. J Mater Process Tech 250:280–288
19. Kasuya T, Yurioka N (1993) Carbon equivalent and multiplying factor for hardenability of steel. Weld J 72:263s–268s
20. Jarvis B, Ahmed N (2000) Development of keyhole mode gas tungsten arc welding process. Sci Technol Weld Joi 5(1):1–7
21. Yudodibroto B (2010) Liquid metal oscillation and arc behaviour during welding. Dissertation. Delft University of Technology
22. Li T, Wu C (2015) Numerical simulation of plasma arc welding with keyhole-dependent heat source and arc pressure distribution. Int J Adv Manuf Technol 78(1–4):593–602
23. Narita K, Takagi K, Kimura T, Mitsui A (1975) Plasma arc welding of pipelines: a study to optimise welding conditions for horizontal fixed joints of mild steel pipes. Int J Pres Ves Pip 3(4):233–266
24. Waszink JH (1983) Experimental investigation of the forces acting on a drop of weld metal. Weld J 62:108s–116s
25. Lago F, Gonzalez J, Freton P, Gleizes A (2004) A numerical modelling of an electric arc and its interaction with the anode: part I. The two-dimensional model. J Phys D Appl Phys 37(6):883–897
26. Ding F, Zi-Cheng H, Jian-Kang H, Xin-Xin W, Yong H (2015) Three-dimensional numerical analysis of interaction between arc and pool by considering the behavior of the metal vapor in tungsten inert gas welding. Acta Phys Sin 64(10):1–11
27. Magudeeswaran G, Balasubramanian V, Reddy GM (2014) Effect of welding processes and consumables on fatigue crack growth behaviour of armour grade quenched and tempered steel joints. Def Technol 10(1):47–59
28. Zhou Y, Jia T, Zhang X, Liu Z, Misra R (2015) Microstructure and toughness of the CGHAZ of an offshore platform steel. J Mater Process Tech 219:314–320
29. Lan L, Qiu C, Zhao D, Gao X, Du L (2011) Microstructural characteristics and toughness of the simulated coarse grained heat affected zone of high strength low carbon bainitic steel. Mater Sci Eng A 529:192–200
30. Zhou T, Yu H, Wang S (2016) Effect of microstructural types on toughness and microstructural optimization of ultra-heavy steel plate: EBSD analysis and microscopic fracture mechanism. Mater Sci Eng A 658:150–158